Classical analog of Stückelberg interferometry in a two-coupled-cantilever–based optomechanical system

Hao Fu,[1] Zhi-cheng Gong,[1] Tian-hua Mao,[1] Chang-pu Sun,[2,3] Su Yi,[4] Yong Li,[2,3,*] and Geng-yu Cao[1,†]

[1]*State Key Laboratory of Magnetic Resonance and Atomic and Molecular Physics, Wuhan Institute of Physics and Mathematics, Chinese Academy of Sciences, Wuhan 430071, People's Republic of China*

[2]*Beijing Computational Science Research Center, Beijing 100193, China*

[3]*Synergetic Innovation Center of Quantum Information and Quantum Physics, University of Science and Technology of China, Hefei, Anhui 230026, China*

[4]*Institute of Theoretical Physics, Chinese Academy of Sciences, Beijing 100190, China*

(Received 7 May 2016; published 31 October 2016)

We present the realization of a Stückelberg interferometer with two mechanical modes in a two-coupled-cantilever–based optomechanical system. By optically tuning the frequency of one cantilever inside a cavity, we show that nonadiabatic crossing of the mechanical modes twice creates the interference fringes of the mechanical oscillations as a result of coherent splitting and subsequent recombination of the oscillations. By measuring the nonadiabatic phase acquired at the transition, we unveil an in-depth analog between the two-mode and quantum two-level systems. With this interferometry-based technique, transferring of oscillation between spatially separated cantilevers is achieved with 97% efficiency.

DOI: 10.1103/PhysRevA.94.043855

I. INTRODUCTION

Following the rapid development in nanofabrication, a mechanical resonator has been used as a universal transducer for direct coupling of mechanical oscillation to various systems ranking from nuclear spins to artificial atoms [1–6]. Moreover, by coupling the mechanical oscillation to the optical field inside a cavity, recent studies in the optomechanical systems have demonstrated the strong capacity of cooling mechanical resonators deep into quantum regime [7,8], which spurs an intensive interest in further realizing a coupled-mechanical-resonator–based multimode optomechanical system for its highly prospective applications on quantum transducers and networks to transfer information between isolated quantum systems [9,10]. With the hybridization of mechanical modes being realized in various optomechanical systems [11–14], optically mediated transfer of oscillation between mechanical modes and especially spatially localized resonators has become of great significance.

It has been demonstrated that coupled resonators of either two mechanical modes [15,16] or cavity modes [17–19] behave as a classical analog of a quantum two-level system, in which coherent manipulation of the energy or even quantum states between two modes has been achieved through the Rabi-like oscillation. Benefitting from strong dispersive optomechanical coupling in a membrane-inside optomechanical system [20–23], coherent transfer of oscillation has been achieved optomechanically recently via the Rabi-like oscillation [14], in which exchange of oscillation energy between two normal modes of a membrane is demonstrated by optically mediating the modes hybridization. Alternative approaches of equal importance involve constructing a Mach-Zender type interferometer by nonadiabatic crossing of mechanical resonances twice [24,25]. It has shown that a classical analog of the Landau-Zener (LZ) transitions can be realized by driving the two mechanical modes of a single nanomechanical beam through the avoid crossing [26]. For a double-passage transition, the first passage coherently splits mechanical oscillations between two resonators and the second one creates their superpositions in both resonators through recombination. As a result, a double-passage process leads to the well-known Stückelberg oscillation, an interference fringe in time domain [27]. Very recently, the classical Stückelberg interferometry between two flexural modes of the single electromechanical resonator has been experimentally realized by Seitner *et al.* [28].

In this work we report the realization of a Stückelberg interferometer in a two-coupled-cantilever–based optomechanical system. Focusing on the fundamental flexural mode of each cantilever, the frequency of one of these modes can be tuned by placing the corresponding cantilever inside a fiber-based Fabry-Pérot cavity and time-resolvedly controlling the pumping power of the cavity. To facilitate the construction of the Stückelberg interferometer, we first demonstrate a coherent splitter for mechanical oscillation via the Landau-Zener-like transition. And then the effective coupling strength between cantilevers is investigated via the Rabi-like oscillation. Finally, we realize the Stückelberg interferometer by driving the system over the avoided crossing twice and obtain the interference fringes of the mechanical oscillations. More interestingly, through the Stückelberg interference, we also determine the nonadiabatic Stokes phase accumulated in the Landau-Zener transitions, which, to the best of our knowledge, has never been measured in a classical system.

II. TUNABLE TWO-MODE OPTOMECHANICAL SYSTEM

As illustrated in Fig. 1(a), the system under investigation consists of two microcantilevers, which are elastically coupled by connecting to the same thin overhang extended $20 \pm 5\ \mu$m out the insulator substrate [13]. Here we focus on the fundamental flexural modes originating from the displacement x_i $(i = 1,2)$ of the cantilevers. In order to tune

*Corresponding author: liyong@csrc.ac.cn
†Corresponding author: gycao@wipm.ac.cn

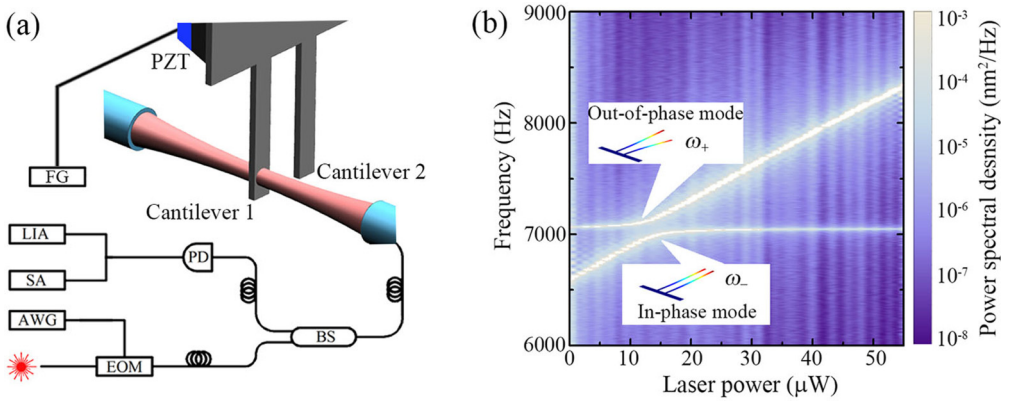

FIG. 1. (a) Schematic drawing of a two-coupled-cantilever–based two-mode optomechanical system. The coupled mechanical resonators consist of two 220-μm-long, 10-μm-wide, and 220-nm-thick single-crystal-silicon cantilevers with a separation of 15 μm. A piezoactuator attached to the substrate of the cantilevers is driven by a function generator (FG) to excite selected mechanical modes. Light inside the 4.5-mm-long fiber cavity is focused by a microlens to the waist radius of 3 μm in the middle. The reflected light is measured by a photodetector (PD) after a 10 db beam splitter (BS). The magnitudes of the signal are subsequently measured by lock-in amplifiers (LIAs) for the oscillation amplitudes of cantilevers. (b) Oscillation power spectral density of the coupled cantilevers versus laser power. The two resonances correspond to the in-phase and out-of-phase motions of the coupled cantilevers as shown in the insets.

the intrinsic frequency of cantilever 1, we insert it into a fiber-based cavity [Fig. 1(a)]; the cavity is then pumped from one side by a 1064 nm Nd-YAG laser with the laser power P. In this configuration the fibers and cantilever 1 form a membrane-in-the-middle optomechanical system, in which the dispersive coupling between the cantilever and the cavity field gives rise to a harmonic trapping to the cantilever corresponding to an effective frequency $\sqrt{gP}$, where g is the optical trapping strength [21]. Consequently, the effective frequency of cantilever 1 $\omega_1(P) = \sqrt{\omega_1^2(0) + gP}$ becomes laser-power dependent, where $\omega_1(0)$ is the intrinsic frequency of cantilever 1 in the absence of pumping laser; while the intrinsic frequency of cantilever 2 ω_2 remains unaffected. Furthermore, the coupling between the cantilevers through the motion-induced stress inside the overhang results in the hybridization of the two fundamental flexural modes and gives rise to two normal modes X_α ($\alpha = +,-$) which are linear combinations of x_1 and x_2. Correspondingly, the frequencies of these normal modes are denoted as $\omega_+(P)$ for the out-of-phase mode and $\omega_-(P)$ for the in-phase mode [Fig. 1(b)].

When the laser power is swept, the avoided crossing of the two normal modes is mapped out in the thermal oscillation spectrum of cantilevers [Fig. 1(b)], in which a minimal frequency splitting of $\Delta/2\pi = 156.8$Hz is observed at the laser power $P_{\rm AC} = 12.9$ μW. Due to the inhomogeneous etching of the substrate, the intrinsic frequencies of cantilevers are different even though their geometrics are essentially the same. It can be further determined from the normal-mode spectrum that the intrinsic frequencies of the cantilevers and the optical trapping strength are, respectively, $\omega_1(0)/2\pi = 6600$ Hz, $\omega_2/2\pi = 7069$ Hz, and $g/(2\pi)^2 = 4.72 \times 10^5$ Hz$^2/\mu$W. Also, in order to obtain Fig. 1(b), the cavity length is tuned such that the mechanical damping rates of the normal modes are independent of the laser power [29]. In fact, it is measured that both the normal modes have essentially the same damping rate $\gamma/2\pi = 3.85$ Hz, which clearly indicates that the system is in the strong coupling regime as $\gamma \ll \Delta$ is satisfied.

III. LANDAU-ZENER-LIKE TRANSITIONS OF MECHANICAL OSCILLATIONS

The two-mode optomechanical system under consideration is analogous to a quantum spin-1/2 system subjected to a longitudinal magnetic field $\varepsilon(P) \equiv \omega_1(P) - \omega_2$ and a transverse magnetic field Δ. Therefore, driving a classical two-mode system through the avoided crossing may also induce a Landau-Zener-like transition of mechanical oscillations between different normal modes [26]. The experimental sequence for demonstrating such a transition is depicted in Fig. 2(a). For the initial state preparation, in order to overcome the cantilevers' thermal motions which have amplitudes around 1 nm at 298 K, we resonantly excite the system with the target mode for 0.45 s until a stable oscillation with amplitude around 90 nm is generated. Here the in-phase mode is actuated at the laser power $P_0 = 0.66$ μW such that about 98% of the mechanical energy is initialized to cantilever 1. Immediately after the initial state preparation ($t = 0$), an arbitrary waveform generator (AWG) is programmed to drive the electro-optical modulator (EOM) such that the power of the pumping laser ramp linearly to $P_f = 54.0$ μW within time t_f. The fast decay of the low-finesse cavity ensures instantaneous change of optomechanical interaction as the laser power is swept. This process may lead to part of the mechanical energy transferring from the in-phase mode to the out-of-phase mode. Here the LZ transition probability is the fraction of the mechanical energy transferred from the in-phase mode to the out-of-phase mode, i.e., $p_{\rm LZ} = A_+(t_f)^2/A_-(0)^2$, where A_α is the amplitude of the αth normal mode. Figure 2(b) shows the transition probability $p_{\rm LZ}$ as a function of the sweeping rate $\upsilon \equiv \frac{d\varepsilon(P)}{dt}|_{P=P_{\rm AC}}$, which is defined at the avoided crossing. As can be seen, the measured transition probability ranges from zero to unit, indicating that, by tuning the sweeping rate, the coupled cantilevers allow adiabatic transfer, coherent splitting, and diabatic transfer for the oscillation state. In particular, a 50/50 splitting is achieved at the sweeping rate $\upsilon/2\pi = 342$ kHz/s. More remarkably, as shown in Fig. 2(b), the transition probability also satisfies the standard LZ formula $p_{\rm LZ} = \exp(-\pi\Delta^2/2|\upsilon|)$, which justifies

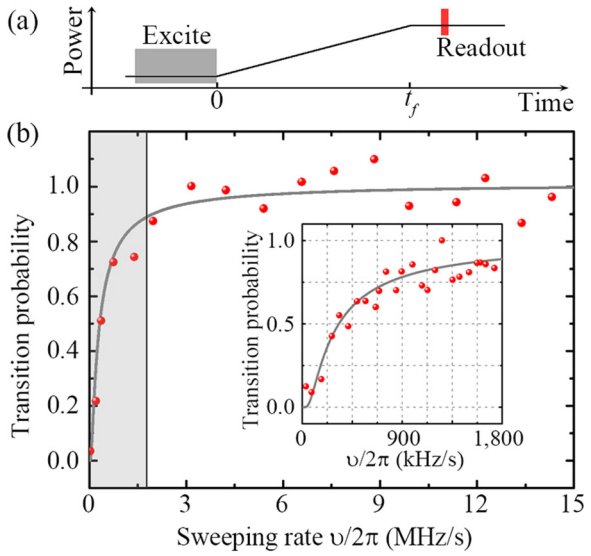

FIG. 2. LZ transition between mechanical modes. (a) Optical driving scheme. After a single passage transition, the laser power is held for optical readout of mechanical oscillations. (b) Transition probability of mechanical oscillations versus sweeping rate. Theoretical result (gray line) calculated from the standard LZ formula is plotted together with the experimental measurement (red dots). The shaded region is shown in detail in the inset.

it as a classical analogy of the LZ transition. In principle, the energy transfer between the spatially separated cantilevers can be achieved via the Landau-Zener transition. However, it requires the adiabatic process with slow sweeping rate of the laser power and thus the transfer efficiency will suffer from the large dissipation (see the Appendix).

IV. RABI OSCILLATION OF THE COUPLED CANTILEVERS

Before constructing the Stückelberg interferometer, we shall first investigate the coupling of cantilevers via the Rabi oscillation. To this aim, as shown in Fig. 3(a), we initialize the system by exciting the in-phase mode at $P_0 = 45.5\ \mu$W, where $\omega_-(P_0) \approx \omega_2$. As a result, almost all of the oscillation energy is localized in cantilever 2. We then linearly ramped down the laser power to the coupling regime P_f within 15 μs, which concludes the state preparation. Here, since the time used to ramp down the laser power is much smaller than $2\pi/\omega_-(P_0)$, the oscillation energy of the initial state remains being localized in cantilever 2. We then hold the laser power at P_f and allow the system to evolve for time τ. Finally, the oscillation amplitude of cantilever 2, $A_2(\tau)$, or equivalently $A_-(\tau)$, is measured 15 ms after we quickly ramp the laser power back to P_0.

In Fig. 3(b) the Bloch sphere shows the states of the system at selected times. In the context of the quantum spin-1/2 model, the physical process can be understood as follows. The initial state is prepared under a sufficiently large longitudinal magnetic field $\varepsilon(P)$ such that the direction of the total magnetic field X_- is roughly along the x_2 axis. By ramping down the laser power to P_f in the coupling regime, we lower the longitudinal magnetic field at time $t = 0$, which effectively

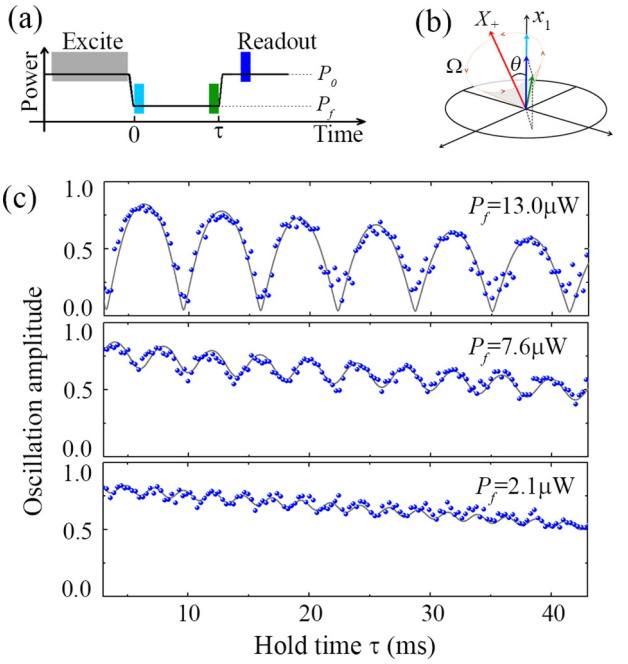

FIG. 3. Rabi oscillation. (a) Optical driving scheme. (b) The Bloch vectors showing the states of the system in the Bloch sphere [marked in the same color in (a)] at selected times. (c) Rescaled oscillation amplitudes of cantilever 2 versus τ for various P_f. Measured data are shown as dots and the fit with Eq. (1) is plotted as solid lines.

deviates X_- from the x_2 axis with angle θ determined by $\tan\theta = \Delta/\varepsilon(P)$ (see the Appendix). After the initialization, the state of the system starts to precess around the X_- axis with the Rabi frequency $\Omega_R = \sqrt{\Delta^2 + \varepsilon^2} = \omega_+ - \omega_-$ such that it becomes a superposition of the oscillations of the two cantilevers. Here the superposition amplitude for the ith cantilever is directly related to the oscillation energy on that cantilever and thus can be determined by measuring the oscillation amplitude A_i after quickly ramping the laser power back to P_0 where two cantilevers are decoupled.

Figure 3(c) plots the measurements of the rescaled oscillation amplitude $A_2(\tau)/A_2(0)$ for various P_f's. As can be seen, a nearly completely transfer of oscillation between cantilevers is achieved when P_f approaches $P_{\rm AC}$, which reflects the fact that the stronger coupling leads to more intensive exchange. While holding the system far from the avoided crossing, however, the weak hybridization of cantilevers outside the coupling region leads to an insufficient exchange of energy. With the power P_f decreasing to 2.1 μW, unobvious Rabi oscillation indicates that the coupling between cantilevers becomes trivial. To gain more insight into the dynamics, we note that the oscillation amplitude of cantilever 2 is governed by the equation (see the Appendix)

$$\frac{A_2(\tau)}{A_2(0)} = e^{-\tau/(2T_d)}\sqrt{1 - \sin^2\theta \sin^2\frac{(\omega_+ - \omega_-)\tau}{2}}. \qquad (1)$$

Here we have phenomenologically included the characteristic decoherence time T_d, which includes the effects of oscillation relaxation and pure dephasing [15]. By fitting the data in Fig. 3(c) with Eq. (1), it is found that $T_d = 37.9$ ms.

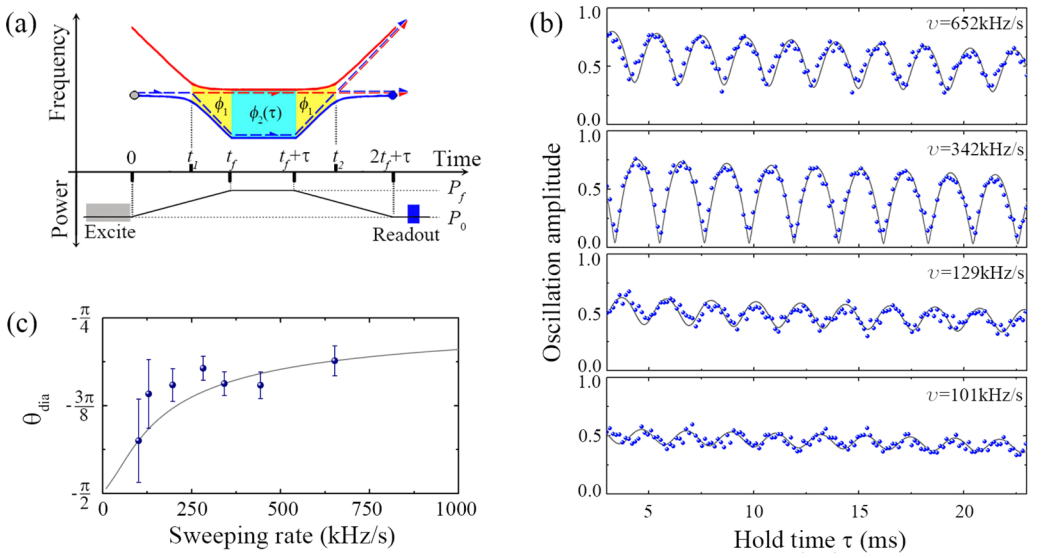

FIG. 4. Stückelberg interferometry of mechanical oscillations. (a) Optical driving scheme and the corresponding adiabatic energy levels. The final mechanical oscillations are then determined as a function of the acquired adiabatic phase $\phi_{\rm adia}(\tau) = \phi_1 + \phi_2(\tau) + \phi_1$ for two normal modes. (b) Interferometer fringes for various sweeping rates. Measured data are shown as dots and the fit with Eq. (2) is plotted as solid lines. (c) Nonadiabatic phases for various sweeping rates. Experimental results (dots) obtained from fitting of the Stückelberg oscillation in (b) are plotted with calculated results (solid line) using the formula of Stokes phase in the text.

V. CLASSICAL ANALOG OF STÜCKELBERG INTERFEROMETRY

The investigations on the LZ transition and Rabi oscillations of the two-mode optomechanical system allow us to study the Stückelberg interferometry based on two subsequent passages through the avoided crossing. Specifically, as illustrated in Fig. 4(a), after exciting the in-phase mode at $P_0 = 55.0\ \mu$W, we linearly ramp down the laser power to $P_f = 0.15\ \mu$W in time t_f such that the avoided crossing is passed through. This process acts as a tunable "beam splitter" which, depending on a sweeping rate υ, allows adiabatic transfer, coherent splitting, and diabatic transfer for the oscillation state. In particular, as shown previously, a 50/50 splitting is achieved with $\upsilon/2\pi = 342$ kHz/s. After the ramp, the laser power is kept constant at P_f for a variable hold time τ. Since the system is outside the coupling region at $P_f = 0.15\ \mu$W, only a differential phase $\phi_{\rm adia}(\tau)$ between the lower and upper states (normal modes) is accumulated. Clearly $\phi_{\rm adia}$ linearly increases with the hold time τ. The laser power is then ramped back up to P_0, and the second passage creates a new superposition state of the upper and lower states depending on $\phi_{\rm adia}$. Here, in analog to a Mach-Zender interferometer, this final step coherently recombines the oscillations leading to the constructive or destructive interference of the oscillation state in the two cantilevers and thus to fringes as a function of τ. Figure 4(b) shows the rescaled oscillation amplitudes $A_2(2t_f + \tau)/A_2(0)$ as a function of hold time τ for various sweeping rates. As can be seen, for the 50/50-splitting ratio we obtain the interference fringes with visibilities as high as 0.94, which indicate the coherence of mechanical oscillation is well preserved in our Stückelberg interferometer.

Our experiment of Stückelberg interferometry shows that the long coherence of mechanical oscillation as well as the reduced dissipation in nonadiabatic operation ensures transferring of mechanical energy between spatially separated cantilevers at the efficiency of 97%, which is obviously better than the transfer efficiency with the adiabatic LZ transition. We note that although similar energy transfer efficiency can also be achieved via the Rabi oscillation, the interferometry-based technique can effectively avoid the unwanted pulsed optomechanical effects [30,31] appearing in the Rabi oscillation.

Quantitatively, the Stückelberg interferometry can be understood in terms of the adiabatic-impulse model [27], which assumes that the system evolves adiabatically unless at the avoided crossing where the LZ transition occurs. Based on this theory, the rescaled oscillation amplitude of cantilever 2 after the double-passage LZ transition takes the form

$$\frac{A_2(2t_f+\tau)}{A_2(0)} = e^{-(2t_f+\tau)/2T_d}\sqrt{1-4p_{\rm LZ}(1-p_{\rm LZ})\cos^2\Phi_{\rm St}}, \tag{2}$$

where $\Phi_{\rm St} = \phi_{\rm adia}(\tau) + \phi_{\rm dia}$ is the Stückelberg phase with $\phi_{\rm adia}(\tau) = \frac{1}{2}\int_{t_1}^{t_2}(\omega_+ - \omega_-)dt$ being the adiabatic phase accumulated during the adiabatic evolution between $t = t_1$ and $t = t_2$ and $\phi_{\rm dia}$ is the phase acquired during the nonadiabatic transitions. Here we have still phenomenologically included the decoherence effect. Quantum mechanically, it is shown that the nonadiabatic phase is $\phi_{\rm dia} = \phi_S - \frac{\pi}{2}$, with $\phi_{\rm S} = \delta(\ln\delta - 1) + \arg[\Gamma(1 - i\delta)] + \frac{\pi}{4}$ being the Stokes phase, here $\delta = \frac{\Delta^2}{4\upsilon}$ and $\Gamma(z)$ is the gamma function [32]. Since $\phi_{\rm adia}(\tau)$ can be evaluated analytically for the given experimental parameters, we may, as shown in Fig. 4(b), determine $\phi_{\rm dia}$ by fitting the measured data with Eq. (2). With the state-of-the-art classical Stückelberg interferometer, in Fig. 4(c) we present the experimentally obtained nonadiabatic phases for various sweeping rates, which are in good agreement with those calculated using the Stokes phase. Unlike the adiabatic phase that is of the dynamic nature, the Stokes phase of

the LZ transition represents the phase acquired during the nonadiabatic transition. With a single passage through the avoided crossing of a two-level system, i.e., the LZ transition, one can determine the occupation probability on each level; while the relative phase between them is often difficult to measure. Although the Rabi oscillation manifests the phase coherence in the dynamics of the coupled cantilevers, no nonadiabatic phase is involved. Therefore, the measurement of the Stokes phase unveils an in-depth analog between the two-mode system and quantum two-level one.

VI. CONCLUSION

In conclusion, we have constructed the Stückelberg interferometer using two coupled cantilevers, demonstrating the classical analog of the Stückelberg interferometer in quantum two-level systems. The nonadiabatic Stokes phase accumulated in the single-passage Landau-Zener transitions has been measured through the Stückelberg interference in our classical system of two coupled cantilevers. We have shown that, utilizing Stückelberg interference, the transfer efficiency of the mechanical oscillation between two spatially separately cantilevers can be as high as 97% with controllable dissipation. Moreover, the achieved high efficient coherent transfer of mechanical oscillation might provide a new optomechanical strategy for further steering information and energy in coupled-resonator–based phononic quantum networks [9,10]. It would also provide a method for enabling optimal generation of nonclassical two-mode squeezed or entangled states for mechanical resonators by modifying time dependently the laser power appropriately.

ACKNOWLEDGMENTS

This work was supported by the National Basic Research Program of China (Grant No. 2012CB922104), and National Natural Science Foundation of China (Grants No. 11121403, No. 11434011, No. 11422437, No. 11204357, and No. U1530401). We thank Wen-xian Zhang, Li-bin Fu, and Yan-jun Ji for helpful discussions and Jia-dong Li for fabricating the coupled cantilevers.

APPENDIX

1. Theoretical model

In the absence of the mechanical excitation, the equations of the motion of the two-mode optomechanical system under consideration can be expressed as

$$\begin{pmatrix} \frac{d^2}{dt^2}+\gamma_1\frac{d}{dt}+\omega_1^2(P) & J \\ J & \frac{d^2}{dt^2}+\gamma_2\frac{d}{dt}+\omega_2^2 \end{pmatrix}\begin{pmatrix} x_1 \\ x_2 \end{pmatrix} = \frac{1}{m}\begin{pmatrix} F_1 \\ F_2 \end{pmatrix}, \tag{A1}$$

where x_i is the displacement of the ith$(I = 1,2)$ cantilever, m is the mass for both the cantilevers, ω_2 $[\omega_1(P)]$ is the intrinsic (optically trapped effective) frequency for the second (first) cantilever, J is the coupling strength between the cantilevers, and F_i is the thermal Brownian force.

Diagonalizing the above equations with neglecting the effects of the damping and noises, we can obtain the out-of-phase (X_+) and an in-phase (X_-) motions of the normal modes $\binom{X_+}{X_-} = U\binom{x_1}{x_2}$, where the transformation matrix $U \equiv U(P)$ represents the contributions of the cantilevers to the normal modes with the explicit form

$$U = \begin{pmatrix} u_{+1} & u_{+2} \\ u_{-1} & u_{-2} \end{pmatrix} = \begin{pmatrix} \cos\frac{\theta}{2} & \sin\frac{\theta}{2} \\ -\sin\frac{\theta}{2} & \cos\frac{\theta}{2} \end{pmatrix}, \tag{A2}$$

Where θ satisfies $\tan\theta = \frac{2J}{\omega_1^2-\omega_2^2}$.

With the above process, Eq. (A1) can be written in the normal-mode motions as

$$\ddot{X}_+ + \omega_+^2\dot{X}_+ = 0, \quad \ddot{X}_- + \omega_-^2\dot{X}_- = 0, \tag{A3}$$

where $\omega_+(P)$ and $\omega_-(P)$ are the eigenfrequencies of the normal modes and

$$\omega_\pm^2 = \tfrac{1}{2}\left[\omega_1^2+\omega_2^2 \pm \sqrt{\left(\omega_1^2-\omega_2^2\right)^2+4J^2}\right]. \tag{A4}$$

Note that the minimal frequency splitting between the normal modes $\Delta := \varepsilon(P_{\rm AC}) = \omega_+(P_{\rm AC}) - \omega_-(P_{\rm AC})$ happening at the energy avoided crossing with the laser power $P_{\rm AC}$ and $\omega_1(P_{AC}) = \omega_2$, is approximately proportional to the coupling strength $\Delta \approx J/\omega_2$ when $J \ll \omega_1^2 \approx \omega_2^2$. Thus, one has $\tan\theta \approx \frac{\Delta}{\omega_1(P)-\omega_2} = \frac{\Delta}{\varepsilon(P)}$.

For a fixed trapping laser power P (which means ω_1 and $\omega_\pm$ are time independent), the time dependence of the normal modes can be generally expressed as

$$X_\pm(t) \equiv \tfrac{1}{2}\tilde{X}_\pm(t) + \text{c.c.} = \tfrac{1}{2}\tilde{A}_\pm e^{-i\omega_\pm t} + \text{c.c.}, \tag{A5}$$

where $\tilde{X}_\pm(t) = \tilde{A}_\pm e^{-i\omega_\pm t}$ represent the corresponding positive-frequency components with $|\tilde{X}_\pm(t)| = |\tilde{A}_\pm| =: A_\pm$ being the (constant) amplitudes of motions of the normal modes. Namely, the corresponding dynamics of (the positive-frequency components of) the normal modes starting from the initial time instant $t_0 = 0$ is subject to a free evolution

$$\begin{pmatrix} \tilde{X}_+(t) \\ \tilde{X}_-(t) \end{pmatrix} = N(t)\begin{pmatrix} \tilde{X}_+(0) \\ \tilde{X}_-(0) \end{pmatrix}, \tag{A6}$$

with the free-evolution matrix

$$N(t) = \begin{pmatrix} e^{-i\omega_+ t} & 0 \\ 0 & e^{-i\omega_- t} \end{pmatrix}. \tag{A7}$$

Similarly, the motions of the cantilevers can be given in the form

$$x_j(t) := \tfrac{1}{2}\tilde{x}_j(t) + \text{c.c.} := \tfrac{1}{2}\tilde{A}_j(t)e^{-i\omega_j t} + \text{c.c.}, \tag{A8}$$

where $\tilde{x}_j(t) = \tilde{A}_j(t)e^{-i\omega_j t}$ $(j = 1,2)$ represents the corresponding positive-frequency components for the jth cantilevers with $|\tilde{x}_j(t)| = |\tilde{A}_j(t)| =: A_j(t)$ being the (time-dependent) amplitudes of motions of the jth cantilever (when the coupling strength is much weaker compared with the eigenfrequencies $J \ll \omega_{1,2}^2$, which is fulfilled for most cases of coupled resonators). Accordingly, the solutions for the motions of the cantilevers can be given as

$$x_j(t) = \tfrac{1}{2}(u_{j+}\tilde{A}_+e^{-i\omega_+ t} + u_{j-}\tilde{A}_-e^{-i\omega_- t}) + \text{c.c.} \tag{A9}$$

according to the solutions of the normal modes' motions.

We would like to point out that when the laser power P is time dependent, the above (constant) amplitudes for the normal

modes $A_\pm$ would be time dependent as $A_\pm(t)$. Meanwhile, the above $N(t)$ would be generalized to be the form

$$N(t,t_0)=\begin{pmatrix} e^{-i\int_{t_0}^{t}\omega_+(t')dt'} & 0 \\ 0 & e^{-i\int_{t_0}^{t}\omega_-(t')dt'} \end{pmatrix}. \quad \text{(A10)}$$

2. Rabi-like oscillations

As demonstrated by Fig. 3 and its related description, when the system is held in the coupling region with the fixed P_f after the initial preparation, the coupling between the cantilevers allow coherent mechanical transferring from cantilevers 2 to 1 following the Rabi-like oscillations. Such an oscillation starting from $t=0$ can be described analytically by the evolutions of the motions of $x_{1,2}(t)\equiv \frac{1}{2}\tilde{x}_{1,2}(t)+\text{c.c.}$, with the positive-frequency components satisfying

$$\begin{pmatrix}\tilde{x}_1(t)\\ \tilde{x}_2(t)\end{pmatrix}=R(t)\begin{pmatrix}\tilde{x}_1(0)\\ \tilde{x}_2(0)\end{pmatrix}. \quad \text{(A11)}$$

Here the newly defined operators

$$R(t)=U^{-1}(P_t)N(t)U(P_t)=\begin{pmatrix}\cos^2\frac{\theta}{2}e^{-i\omega_+t}+\sin^2\frac{\theta}{2}e^{-i\omega_-t} & \cos\frac{\theta}{2}\sin\frac{\theta}{2}(e^{-i\omega_-t}-e^{-i\omega_+t})\\ \cos\frac{\theta}{2}\sin\frac{\theta}{2}(e^{-i\omega_-t}-e^{-i\omega_+t}) & \sin^2\frac{\theta}{2}e^{-i\omega_+t}+\cos^2\frac{\theta}{2}e^{-i\omega_-t}\end{pmatrix} \quad \text{(A12)}$$

represents the operation of the Rabi-like oscillations for the positive-frequency parts of the motions of the cantilevers with $U(P_t)$ the corresponding mode function. And $N(t)=\left(\begin{smallmatrix} e^{-i\omega_+t} & 0\\ 0 & e^{i\omega_-t}\end{smallmatrix}\right)$ denotes the free evolution for the normal-mode basis $\{X_\pm\}$ for a fixed laser power. Namely, the evolution of the mechanical oscillations transferring between the cantilevers in the coupling region can be resorted to the free evolution for the normal modes sandwiched by the two related mode-function transformations.

In the case of Fig. 3, after the excitation for cantilever 2 (in-phase normal mode), the trapping power is ramped linearly to P_f in a very short time interval with the fast sweeping limit. That means the initial values for the Rabi-like oscillation of the cantilevers are approximately the excitation ones: $|\tilde{x}_2(0)|=A_2(0)\gg|\tilde{x}_1(0)|=A_1(0)\approx 0$. Thus, the (normalized) oscillation amplitudes of the cantilevers after the hold time τ are described analytically as

$$\begin{aligned}\frac{A_1(\tau)}{A_2(0)}&=\frac{|\tilde{x}_1(\tau)|}{|\tilde{x}_2(0)|}=\left|\sin\theta\sin\frac{(\omega_+-\omega_-)\tau}{2}\right|,\\ \frac{A_2(\tau)}{A_2(0)}&=\frac{|\tilde{x}_2(\tau)|}{|\tilde{x}_2(0)|}=\sqrt{1-\sin^2\theta\sin^2\frac{(\omega_+-\omega_-)\tau}{2}}.\end{aligned} \quad \text{(A13)}$$

That means the related Rabi frequency for the Rabi oscillations is $\Omega_R=\omega_+-\omega_-=\sqrt{\Delta^2+\varepsilon^2}$.

3. Stückelberg interferometry

According to the adiabatic-impulse model [27], the Stückelberg interferometry includes three processes: the first Landau-Zener transition, the adiabatical evolution, and the second Landau-Zener transition. In each transition mimicking a coherent oscillation splitter, the transition matrix is given in the positive-frequency part of the normal-mode basis $\{X_\pm\}$ as

$$T=\begin{pmatrix}\sqrt{1-p_{\rm LZ}}\,e^{-i\phi_{\rm dia}} & -\sqrt{p_{\rm LZ}}\\ \sqrt{p_{\rm LZ}} & \sqrt{1-p_{\rm LZ}}\,e^{i\phi_{\rm dia}}\end{pmatrix}, \quad \text{(A14)}$$

with $p_{\rm LZ}$ the transition probability and $\phi_{\rm dia}$ the phase acquired during the nonadiabatic transitions (with their explicit forms given in the main text). During the adiabatic process between the two Landau-Zener transitions, the motions of the normal modes is governed by

$$N(t_2,t_1)=\begin{pmatrix}e^{-i\phi_+(\tau)} & 0\\ 0 & e^{-i\phi_-(\tau)}\end{pmatrix}, \quad \text{(A15)}$$

with $\phi_\pm:=\int_{t_1}^{t_2}\omega_\pm(t)dt$.

Accordingly, one can readily obtain the following motions of the positive-frequency part of the normal modes:

$$\begin{pmatrix}\tilde{X}_+(2t_f+\tau)\\ \tilde{X}_-(2t_f+\tau)\end{pmatrix}=S\begin{pmatrix}\tilde{X}_+(0)\\ \tilde{X}_-(0)\end{pmatrix}, \quad \text{(A16)}$$

with

$$S=TN(t_2,t_1)T:=\begin{pmatrix}S_{11} & S_{12}\\ S_{21} & S_{22}\end{pmatrix}=\begin{pmatrix}(1-p_{\rm LZ})e^{-i(2\phi_{\rm dia}+\phi_+)}-p_{\rm LZ}e^{-i\phi_-} & -\sqrt{p_{\rm LZ}(1-p_{\rm LZ})}[e^{-i(\phi_{\rm dia}+\phi_+)}+e^{i(\phi_{\rm dia}-\phi_-)}]\\ \sqrt{p_{\rm LZ}(1-p_{\rm LZ})}[e^{-i(\phi_{\rm dia}+\phi_+)}+e^{i(\phi_{\rm dia}-\phi_-)}] & (1-p_{\rm LZ})e^{i(2\phi_{\rm dia}-\phi_-)}-p_{\rm LZ}e^{-i\phi_+}\end{pmatrix}. \quad \text{(A17)}$$

Using the conditions $\tilde{x}_1(t)\approx\tilde{X}_+(t),\tilde{x}_2(t)\approx\tilde{X}_-(t)$ for the initial time instant $t=0$ and the final one $t=2t_f+\tau$ (where the system is far away from the avoided crossing) and the initial amplitude conditions $A_2(0)=|\tilde{x}_2(0)|\gg A_1(0)=|\tilde{x}_1(0)|\approx 0$, one can get the (normalized) final amplitudes of the cantilevers as

$$\begin{aligned}\frac{A_1(2t_f+\tau)}{A_2(0)}&=\frac{|\tilde{x}_1(2t_f+\tau)|}{|\tilde{x}_2(0)|}=|S_{12}|=2\sqrt{p_{\rm LZ}(1-p_{\rm LZ})}|\cos\Phi_{\rm St}|,\\ \frac{A_2(2t_f+\tau)}{A_2(0)}&=\frac{|\tilde{x}_2(2t_f+\tau)|}{|\tilde{x}_2(0)|}=|S_{22}|=\sqrt{1-4p_{\rm LZ}(1-p_{\rm LZ})\cos^2\Phi_{\rm St}},\end{aligned} \quad \text{(A18)}$$

where $\Phi_{\rm St} = \phi_{\rm dia} + \phi_{\rm adia}(\tau)$, with $\phi_{\rm adia}(\tau) = \frac{1}{2}[\phi_+(\tau) - \phi_-(\tau)] = \frac{1}{2}\int_{t_1}^{t_2}[\omega_+(t) - \omega_-(t)]dt$ being the adiabatic phase accumulated during the adiabatic evolution. As shown in Fig. 4(a), the adiabatic phase $\phi_{\rm adia}(\tau)$ can be described by the following form $\phi_{\rm adia}(\tau) = \phi_1 + \phi_2(\tau) + \phi_1$, where $\phi_1 = \frac{1}{2}\int_{t_1}^{t_f}[\omega_+(t) - \omega_-(t)]dt$ is the hold time τ independent phase and $\phi_2 = \frac{1}{2}\int_{t_f}^{t_f+\tau}[\omega_+(t) - \omega_-(t)]dt = \frac{1}{2}[\omega_+(P_f) - \omega_-(P_f)]\tau$ is the relevant phase.

4. Numerical simulations

Now we investigate the numerical simulations of the time evolutions for the system of two coupled resonators under consideration by including the effects of the damping and thermal noises. To this aim, we rewrite the equations of the motion (A1) in the form as

$$\begin{aligned}
\dot{x}_1 &= \frac{p_1}{m},\\
\dot{p}_1 &= -m\omega_1^2(P)x_1 - mJx_2 - \gamma p_1 + F_1(t),\\
\dot{x}_2 &= \frac{p_2}{m},\\
\dot{p}_2 &= -m\omega_2^2 x_2 - mJx_1 - \gamma p_2 + F_2(t),
\end{aligned} \tag{A19}$$

where $x_{1,2}$, $p_{1,2}$, m, $\omega_{1,2}$, and γ are, respectively, the positions, momenta, masses, eigenfrequecies, and damping rates of the mechanical resonators. J is the coupling strength between the resonators. Here the thermal Brownian noises $F_{1,2}(t)$ satisfy

$$\langle F_j(t)F_{j'}(t')\rangle = 2k_BTm\gamma\delta_{jj'}\delta(t-t') \tag{A20}$$

($\langle\cdots\rangle$ denotes the ensemble average) in the high-temperature limit $k_BT/(\hbar\omega_{1,2}) \gg 1$ as in our experiment. Here k_B, T, and $\hbar$ are the Boltzmann constant, ambient temperature, and reduced Plank constant, respectively.

In order to include the effects of both the damping and the thermal Brownian noises, here we consider the evolution of the close equations of motion for the mean values of the quadratic terms like x_1^2. Using the equations of motion in Eq. (A19) and the correlation

$$\begin{aligned}
\langle x_j(t)F_{j'}(t')\rangle &= 0,\\
\langle p_j(t)F_{j'}(t)\rangle &= \begin{cases} k_BTm\gamma\delta_{jj'} & (t=t'),\\ 0 & (t\neq t')\end{cases}
\end{aligned} \tag{A21}$$

we can get the following equations of motion:

$$\frac{\partial}{\partial t}\boldsymbol{\mu} = -\mathbf{M}\boldsymbol{\mu} + \boldsymbol{\nu}, \tag{A22}$$

with $\boldsymbol{\mu} = [\langle x_1^2\rangle, \langle x_1p_1\rangle, \langle p_1^2\rangle, \langle x_2^2\rangle, \langle x_2p_2\rangle, \langle p_2^2\rangle, \langle x_1p_2\rangle, \langle x_2p_1\rangle, \langle x_1x_2\rangle, \langle p_1p_2\rangle]^{\rm T}$,

$$\mathbf{M} = \begin{pmatrix}
0 & \frac{-2}{m} & 0 & 0 & 0 & 0 & 0 & 0 & 0 & 0\\
m\omega_1^2 & \gamma & \frac{-1}{m} & 0 & 0 & 0 & 0 & 0 & mJ & 0\\
0 & 2m\omega_1^2 & 2\gamma & 0 & 0 & 0 & 0 & 2mJ & 0 & 0\\
0 & 0 & 0 & 0 & \frac{-2}{m} & 0 & 0 & 0 & 0 & 0\\
0 & 0 & 0 & m\omega_2^2 & \gamma & \frac{-1}{m} & 0 & 0 & mJ & 0\\
0 & 0 & 0 & 0 & 2m\omega_2^2 & 2\gamma & 2mJ & 0 & 0 & 0\\
mJ & 0 & 0 & 0 & 0 & 0 & \gamma & 0 & m\omega_2^2 & \frac{-1}{m}\\
0 & 0 & 0 & mJ & 0 & 0 & 0 & \gamma & m\omega_1^2 & \frac{-1}{m}\\
0 & 0 & 0 & 0 & 0 & 0 & \frac{-1}{m} & \frac{-1}{m} & 0 & 0\\
0 & mJ & 0 & 0 & mJ & 0 & m\omega_1^2 & m\omega_2^2 & 0 & 2\gamma
\end{pmatrix}$$

and $\boldsymbol{\nu} = (0,0,2m\gamma k_BT,0,0,2m\gamma k_BT,0,0,0,0)^{\rm T}$.

According to the above equations (A22), we can obtain numerically the motion of each cantilever at any time instant once we know the initial conditions. For example, in the case of the Landau-Zener transition as given in Fig. 2, the corresponding initial condition is $\boldsymbol{\mu}(0) = [A^2,0,2mk_BT,2k_BT/(m\omega_2^2),0,2mk_BT,0,0,0,0]^{\rm T}$. The related numerical results of the oscillation energies (or the oscillation powers) are in good agreement with the experimental ones and the ones according to the formula of standard Landau-Zener transition, as seen in Fig. 5.

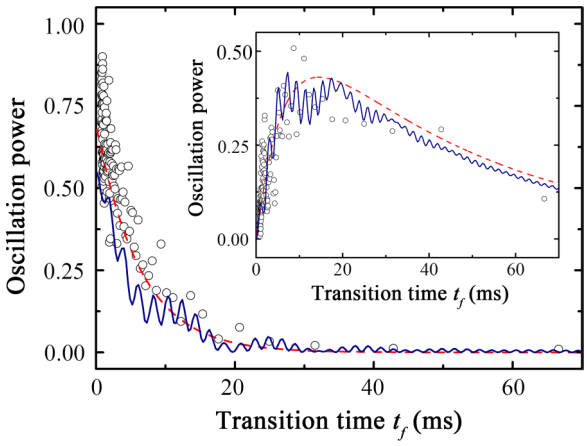

FIG. 5. Oscillation power of cantilevers. The oscillation powers of cantilever 2 and (inset) cantilever 1 are rescaled to the oscillation power of cantilever 2 immediately after the initialization. Experimental results (black circles) and the results calculated from the standard LZ formula considering the mechanical damping (dashed red lines) are plotted in comparison with the related numerical results (solid blue lines). Here the numerical calculations are performed with $m = 1.03$ ng, $T = 298$ K, and all the other parameters the same as those in Fig. 2.

[1] J. Bochmann, A. Vainsencher, D. D. Awschalom, and A. N. Cleland, Nat. Phys. **9**, 712 (2013).
[2] C. L. Degen, M. Poggio, H. J. Mamin, C. T. Rettner, and D. Rugar, Proc. Natl. Acad. Sci. U.S.A. **106**, 1313 (2009).
[3] S. Kolkowitz, A. C. B. Jayich, Q. P. Unterreithmeier, S. D. Bennett, P. Rabl, J. G. E. Harris, and M. D. Lukin, Science **335**, 1603 (2012).
[4] S. Singh, H. Jing, E. M. Wright, and P. Meystre, Phys. Rev. A **86**, 021801 (2012).
[5] B. Vogell, K. Stannigel, P. Zoller, K. Hammerer, M. T. Rakher, M. Korppi, A. Jöckel, and P. Treutlein, Phys. Rev. A **87**, 023816 (2013).
[6] Z.-L. Xiang, S. Ashhab, J. Q. You, and F. Nori, Rev. Mod. Phys. **85**, 623 (2013).
[7] J. Chan, T. P. Alegre, A. H. Safavi-Naeini, J. T. Hill, A. Krause, S. Gröblacher, M. Aspelmeyer, and O. Painter, Nature (London) **478**, 89 (2011).
[8] J. D. Teufel *et al.*, Nature (London) **475**, 359 (2011).
[9] S. J. M. Habraken, K. Stannigel, M. D. Lukin, P. Zoller, and P. Rabl, New J. Phys. **14**, 115004 (2012).
[10] P. Rabl, S. J. Kolkowitz, F. H. L. Koppens, J. G. E. Harris, P. Zoller, and M. D. Lukin, Nat. Phys. **6**, 602 (2010).
[11] Q. Lin, J. Rosenberg, D. Chang, R. Camacho, M. Eichenfield, K. J. Vahala, and O. Painter, Nat. Photon. **4**, 236 (2010).
[12] M. Zhang, G. S. Wiederhecker, S. Manipatruni, A. Barnard, P. McEuen, and M. Lipson, Phys. Rev. Lett. **109**, 233906 (2012).
[13] H. Fu, T.-h. Mao, Y. Li, J.-f. Ding, J.-d. Li, and G. Cao, Appl. Phys. Lett. **105**, 014108 (2014).
[14] A. B. Shkarin, N. E. Flowers-Jacobs, S. W. Hoch, A. D. Kashkanova, C. Deutsch, J. Reichel, and J. G. E. Harris, Phys. Rev. Lett. **112**, 013602 (2014).
[15] T. Faust, J. Rieger, M. J. Seitner, J. P. Kotthaus, and E. M. Weig, Nat. Phys. **9**, 485 (2013).
[16] H. Okamoto, A. Gourgout, C.-Y. Chang, K. Onomitsu, I. Mahboob, E. Y. Chang, and H. Yamaguchi, Nat. Phys. **9**, 480 (2013).
[17] F. Lecocq, J. B. Clark, R. W. Simmonds, J. Aumentado, and J. D. Teufel, Phys. Rev. Lett. **116**, 043601 (2016).
[18] Y. D. Wang and A. A. Clerk, Phys. Rev. Lett. **108**, 153603 (2012).
[19] G. Heinrich, J. G. E. Harris, and F. Marquardt, Phys. Rev. A **81**, 011801 (2010).
[20] M. Bhattacharya, H. Uys, and P. Meystre, Phys. Rev. A **77**, 033819 (2008).
[21] K. K. Ni, R. Norte, D. J. Wilson, J. D. Hood, D. E. Chang, O. Painter, and H. J. Kimble, Phys. Rev. Lett. **108**, 214302 (2012).
[22] J. D. Thompson, B. M. Zwickl, A. M. Jayich, F. Marquardt, S. M. Girvin, and J. G. E. Harris, Nature (London) **452**, 72 (2008).
[23] Z. J. Deng, Y. Li, M. Gao, and C. W. Wu, Phys. Rev. A **85**, 025804 (2012).
[24] W. D. Oliver, Y. Yu, J. C. Lee, K. K. Berggren, L. S. Levitov, and T. P. Orlando, Science **310**, 1653 (2005).
[25] H. Wu, G. Heinrich, and F. Marquardt, New J. Phys. **15**, 123022 (2013).
[26] T. Faust, J. Rieger, M. J. Seitner, P. Krenn, J. P. Kotthaus, and E. M. Weig, Phys. Rev. Lett. **109**, 037205 (2012).
[27] S. N. Shevchenko, S. Ashhab, and F. Nori, Phys. Rep. **492**, 1 (2010).
[28] M. J. Seitner, H. Ribeiro, J. Kölbl, T. Faust, J. P. Kotthaus, and E. M. Weig, arXiv:1602.01034.
[29] With the membrane-in-the-middle configuration, the optomechanical coupling contains two terms that are respectively linear and quadratic in the mechanical displacement [20,22]. Here both coupling coefficients can be tuned through the length of the cavity (i.e., changing the positions of the cavity mirrors). Because the linear (quadratic) coupling is mainly responsible for optical damping (trapping) of the mechanical resonator, the cavity length is tuned such that linear coupling coefficient is negligibly small compared to the quadratic one, which ensures that damping is insensitive to the laser power.
[30] S. M. Meenehan, J. D. Cohen, G. S. MacCabe, F. Marsili, M. D. Shaw, and O. Painter, Phys. Rev. X **5**, 041002 (2015).
[31] M. R. Vanner, I. Pikovski, G. D. Cole, M. S. Kim, C. Brukner, K. Hammerer, G. J. Milburn, and M. Aspelmeyer, Proc. Nat. Acad. Sci. U.S.A. **108**, 16182 (2011).
[32] Y. Kayanuma, Phys. Rev. A **55**, R2495(R) (1997).